Applied Surface Science 283 (2013) 175–180

Contents lists available at SciVerse ScienceDirect

Applied Surface Science

journal homepage: www.elsevier.com/locate/apsusc

Ethanol assisted synthesis of anatase nanobelts with improved crystallinity and photocatalytic activity

Binbin Ni [a], Feng Li [a], Xiaoning Li [a], Zhengping Fu [a,*], Yanwu Zhu [a], Yalin Lu [a,b,c,**]

[a] CAS Key Laboratory of Materials for Energy Conversion, Department of Materials Science and Engineering, University of Science and Technology of China, Hefei, Anhui 230026, PR China
[b] Hefei National Laboratory for Physical Sciences at Microscale, University of Science and Technology of China, Hefei, Anhui 230026, PR China
[c] Laser Optics Research Center, US Air Force Academy, CO 80840, USA

ARTICLE INFO

Article history:
Received 11 April 2013
Received in revised form 4 June 2013
Accepted 5 June 2013
Available online 3 July 2013

Keywords:
TiO_2 nanobelt
Ethanol
Crystallinity
Photocatalytic activity

ABSTRACT

A modified alkaline hydrothermal method via adding the ethanol treatment to the intermediates was developed to synthesize TiO_2 nanobelts, in which the main phase is anatase. Compared with the previous reported TiO_2 nanobelts obtained without the ethanol treatment, the new TiO_2 nanobelts obtained through the ethanol assisted route are with much improved anatase crystallinity and a sharply reduced amount of TiO_2-B phase, as well as a significantly higher photocatalytic activity that is even better than P25 for degrading Rhodamine-B under the ultraviolet light irradiation, which apparently correlates to the increased contents and crystallinity of anatase. The mechanism of ethanol treatment is also discussed based on the FTIR results.

1. Introduction

Deterioration of environmental condition and shortage of natural resources have been attracting considerable public attention during recent years. Titanium dioxide (TiO_2), as a kind of effortlessly available and stable nontoxic semiconductor, has been widely investigated in photocatalysis [1–3], solar cell [4], and Li-ion battery applications [5,6], with a goal to struggle with these intractable problems. Since the pioneer work that Fujishima and Honda found the phenomenon of water splitting by TiO_2 electrodes [7], physicochemical performances of TiO_2 have been found to be highly related to the geometrical morphology, size, degree of crystallinity and the surface structure, and reduction in size to the nanoscale has been the trend of investigation in recent years [8]. However, for the widely studied nanoparticles, benefits from the quantum size effect and the increased reactive sites could be canceled by severe agglomeration and high recombination rates of the photoinduced carriers. Moreover, small sizes of nanoparticles also mean an increase difficulty to recycling them from commonly used aqueous solutions [9], poorer repeatability and then increased costs.

One-dimensional (1D) TiO_2 nanostructures, especially the nanobelts, have been extensively studied due to their relatively stable morphology at high calcination temperature, unique surface atomic arrangement and oriented migration path for photogenerated charge carriers [9–11]. Among various demonstrated approaches to synthesize TiO_2 nanobelts, alkaline hydrothermal method possesses relatively concise preparation steps, low cost and good repeatability [12,13]. The general process in this method contains the phase transformation among $Na_2Ti_3O_7$, $H_2Ti_3O_7$ and TiO_2. Moreover, phase of the resulted TiO_2 nanobelts may include TiO_2-B, anatase and rutile which depend on the subsequent calcination temperature [9,14]. TiO_2-B is an exotic monoclinic polymorph with mesoporous structures which is thought to be an intermediate phase between $H_2Ti_3O_7$ and anatase during the calcinating process [9,15,16]. In general, among all kinds of titania polymorphs, anatase exhibits a better activity than rutile and TiO_2-B [9,17]. However, low calcination temperature may result in a low degree of crystallinity and then a high percentage of TiO_2-B, which will seriously slash the activity of TiO_2 nanobelts. On the other hand, high calcination temperature will induce distortion and fusion of the nanobelts, leading to a low specific area which then decreases the surface active sites [9]. Majority of previous attentions were focused on fabricating bicrystal TiO_2 nanobelts consisting both TiO_2-B and anatase parts [18]. However, photocatalytic activity of the bicrystal TiO_2 nanobelts was still inferior to the commercial TiO_2 nanoparticles (P25) [19,20].

With the goal of finding new ways able to enhance the nanobelts' photocatalytic activity, in this work we developed an

* Corresponding author. Tel.: +86 551 63603194.
** Corresponding author at: CAS Key Laboratory of Materials for Energy Conversion, Department of Materials Science and Engineering, University of Science and Technology of China, Hefei, Anhui 230026, PR China. Tel.: +86 551 63603004.
E-mail addresses: fuzp@ustc.edu.cn (Z. Fu), yllu@ustc.edu.cn (Y. Lu).

0169-4332/$ – see front matter © 2013 Elsevier B.V. All rights reserved.
http://dx.doi.org/10.1016/j.apsusc.2013.06.076

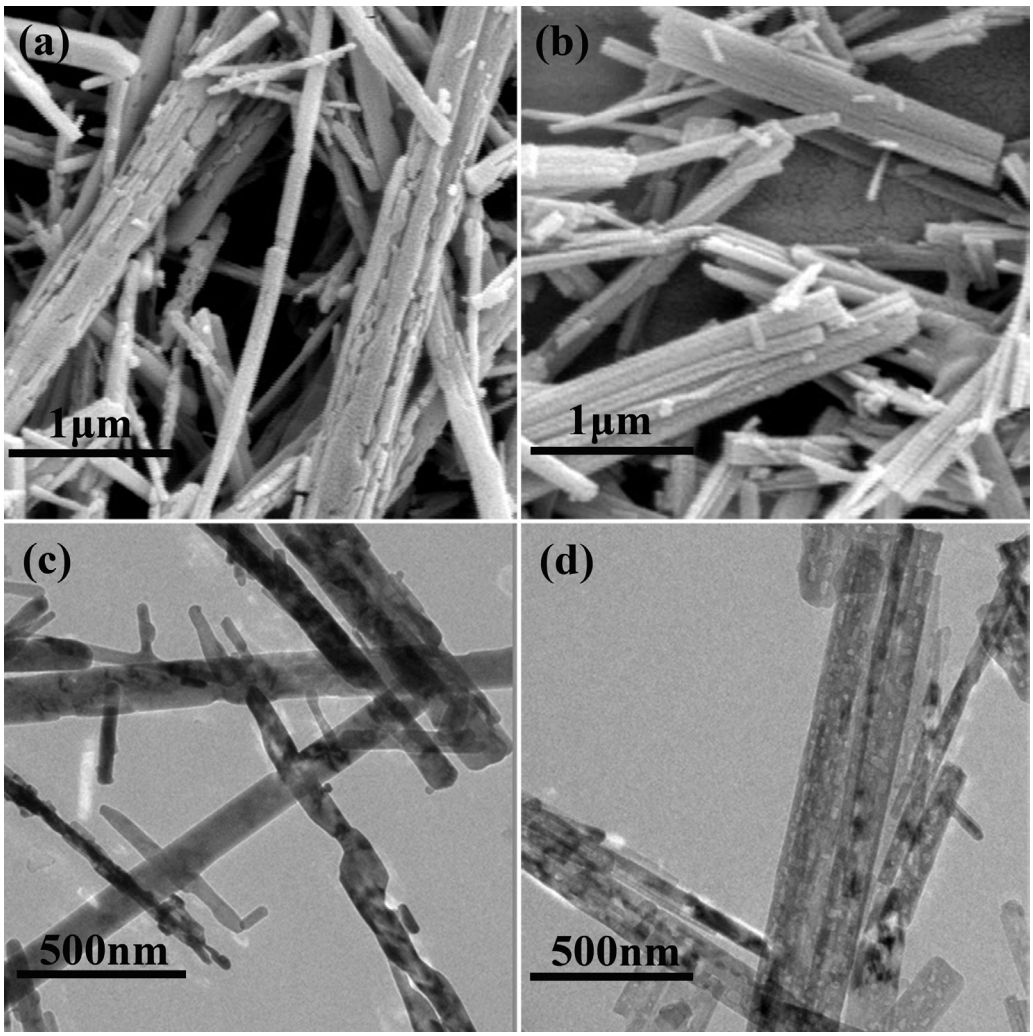

Fig. 1. FESEM images of ANB (a) and TNB (b); TEM images of ANB (c) and TNB (d).

ethanol-assisted alkaline hydrothermal approach. In contrast to the acid assisted approach in some previous researches [18–20], this new process is more convenient and facile, and the resulting products own increased contents and crystallinity of anatase if using the same calcination temperature. The resulting nanobelts show much improved photocatalytic activity that is better than P25 and previous reported TiO_2 nanobelts, when decomposing Rhodamine-B (RB) under the ultraviolet light illumination.

2. Experimental

2.1. Synthesis of TiO_2 nanobelts

Fabrication of TiO_2 nanobelts follows mainly the common alkaline hydrothermal method [11]. 1 g TiO_2 nanoparticles (Degussa P25) powders were dissolved in 80 ml NaOH aqueous solution (10 M) by a continuous magnetic stirring for 1 h. Then the obtained suspension was transferred into a 100 ml Teflon-sealed autoclave and kept at 200 °C for 24 h. The resulting products were rinsed with ultrapure water through vacuum filtration until the pH value reached 8 with soaking in dilute HCl aqueous solution (0.1 M) for 12 h. The samples were eventually washed to neutral to get the $H_2Ti_3O_7$ wet powders. By immersing the as prepared $H_2Ti_3O_7$ wet powders in 50 ml ethanol at room temperature for 0.5 h, the ethanol treated $H_2Ti_3O_7$ (E-$H_2Ti_3O_7$) were obtained. Throughout the paper, the samples obtained by annealing E-$H_2Ti_3O_7$ and $H_2Ti_3O_7$ in air at 600 °C were denoted as ANB and TNB (without the ethanol treatment), respectively. As a contrast, the nanobelts achieved by acid assisted method in previous reports were also obtained which denoted as H-TNB [19,20].

2.2. Characterization

Morphology of the samples was observed by field emission scanning electron microscopy (JSM-6700F). Their crystalline phase was evaluated by a Rigaku-TTR III X-ray diffractometer with Cu-Kα radiation. The lattice structures were obtained by the transmission electron microscopy (TEM, JEM-2010). The specific surface area BET values were acquired by a N_2 adsorption–desorption analyzer (Tristar II 3020M). UV–vis absorption spectra were recorded on a UV-Vis spectrophotometer (SOLID 3700). The Fourier transform infrared spectra (Nicolet 8700) were measured at room temperature by the KBr method.

2.3. Photocatalytic tests

Photocatalysis activities of different samples were investigated by the photo-degradation of Rhodamine-B (RB). In a typical photocatalytic test, 20 mg sample was sonicated in 80 ml of 5 mg/L RB aqueous solution in a 100 ml beaker, and then the solution was

Table 1
BET surface area, pore volume and photocatalytic reaction activity of ANB, TNB, H-TNB and P25.

Sample	S_{bet} (m^2/g)	Pore volume (cm^3/g)	K (min^{-1})	K_0 ($min^{-1}\,m^{-2}\,g^{-1}$)
ANB	16.8	0.0394	0.0220	13.1×10^{-4}
TNB	29.6	0.1109	0.0077	2.6×10^{-4}
P25	49.9	0.3857	0.0185	3.7×10^{-4}
H-TNB	45.2	0.1507	0.0121	2.7×10^{-4}

stirred in the dark for 0.5 h to ensure the adsorption equilibrium. The photocatalytic reaction was started by turning on the 20 W low-pressure Hg lamp with a wavelength range of 320–400 nm, which was positioned 15 cm from the liquid level. At the fixed time intervals, 3 ml suspended solution was extracted and centrifuged to obtain the supernate, which was analyzed to determine the concentration of surplus RB by recording the absorption peak (553 nm) using a UV-Vis spectrometer.

3. Results and discussion

Morphologies of the TiO_2 nanobelts with (ANB) and without (TNB) treatment of ethanol are shown in Fig. 1. Fig. 1a and b displays typical FESEM images of ANB and TNB, respectively. The nanobelts are 50–200 nm in width and several micrometers in length. Some nanobelts are bound together as bundles, which can be attributed to the minimization of interfacial energy among those nanobelts with the same crystallographic orientation [21]. However, comparing with the straight sides of TNB, edges of ANB are partially irregular and corrugate due to the added soaking in ethanol before calcination. The evolutive process of the nanobelts involves a serial of chemical reactions. It starts from the dismantling of the Ti—O—Ti building units of the raw nanoparticles in the alkaline-hydrothermal condition and rearrange to form a six-coordinated monomer subsequently: $[Ti(OH)_6]^{2-}$ [22]. Then plenty of original crystal nucleus are formed due to the combination of $[Ti(OH)_6]^{2-}$ monomers with each other through oxolation and olation [10]. This specific nucleation mechanism results in a preferred orientation growth which lead to the formation of small nanosheets. As the hydrothermal reaction continues, the quasi-1D $Na_xH_{2-x}Ti_3O_7$ nanobelts form gradually. The following acid washing and calcination finally transform the phase to TiO_2 [23]. The TEM images of ANB and TNB are shown in Fig. 1c and d, respectively. From the images, we can observe numerous bubble-like mesoporous with 10–30 nm in diameter are embedded in the major exposed facets of TNB, while the surfaces of ANB are primarily compact and clean. This difference of micro-structure is consistent with the BET values and pore volumes of the two kinds of nanobelts. The BET and pore volume of ANB (16.8 m^2/g, 0.0394 cm^3/g) are both less than those of TNB (29.6 m^2/g, 0.1109 cm^3/g), which are listed in Table 1. In consideration of the mesoporous structure of TiO_2-B [15], the difference of these data may has a correlation with the components change among different phases.

X-ray diffraction results are shown in Fig. 2. The raw material of P25 nanoparticles exhibits the characteristic peaks of anatase (JCPDF 21-1272) and rutile (JCPDF 21-1276). Similar to previous studies, distinct diffraction peaks of anatase and TiO_2-B were clearly observed in TNB. Those weak peaks at 15, 25, 28.5, 29.9, 33.3, 43.5, 44.5 and 48.5° are indexed to TiO_2-B (JCPDF 46-1237). However, by immersing the as prepared $H_2Ti_3O_7$ wet powders in ethanol before calcination, the crystallinity of anatase in the resulted ANB powders was drastically increased, while the phase of TiO_2-B almost disappeared synchronously. Taking the main peak (1 0 1) at 25.3° as the comparative reference, the crystalline degree of anatase for ANB is superior to that of P25, where the full-width at half maximum (FWHM) for the (1 0 1) diffraction peak of ANB

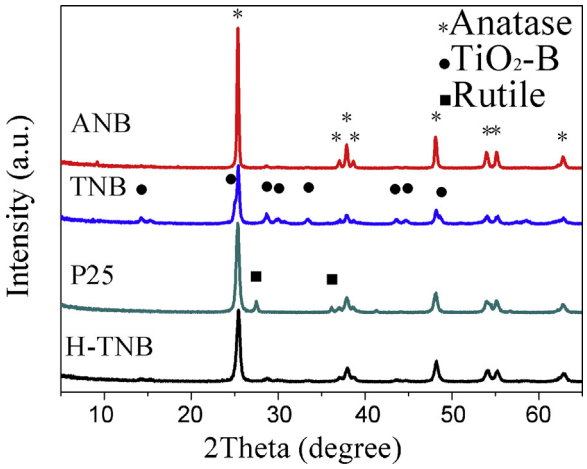

Fig. 2. XRD patterns of ANB, TNB, P25 and H-TNB.

is smaller than that of P25 (0.22° vs 0.42° in 2θ). In addition, it should be noted that the TiO_2 nanobelts with the acid corrosion (H-TNB) also exhibit an improved crystallinity of anatase and a decreased proportion of TiO_2-B relative to TNB. This improvement was explained by the dissolving of $H_2Ti_3O_7$ and the rearrangement of anatase on surfaces of $H_2Ti_3O_7$ nanobelts [20]. However, the increment in the crystallinity improvement of anatase by the acid corrosion is far less than that by soaking in ethanol. Moreover, neutral circumstance and the room-temperature operation of the used ethanol treatment also make the process more appealing in a practical application.

Lattice details can be observed from the HRTEM images given in Fig. 3. The ANB displays (Fig. 3a) large-scale uniform fringes with high contrast. The fringes parallel to the longitudinal direction of the nanobelts with a ca. 0.241 nm lattice spacing can be assigned to the {−1 0 3} planes of anatase. The lattice spacing of the other set of fringes is 0.352 nm, corresponding to the {1 0 1} facets of anatase. The measured angle between the two planes is 71.8°, which is consistent with the theoretical expectation. These complete and distinct crystalline lattices signify that highly crystalline anatase has been fabricated via the ethanol treatment. Fig. 3b shows the HRTEM image of TNB. Lattice spacing of 0.357 nm and 0.352 nm belong to $d_{1\,1\,0}$ of TiO_2-B and $d_{1\,0\,1}$ of anatase, respectively. The blurred fringes of TiO_2-B testify its poor crystallinity, and this can be further evidenced by the increased amount of lattice defects. The crystalline lattice encircled by dashed lines present an edge dislocation which leads to the termination of several planes and deflection of other adjacent planes. Furthermore, another type of planes with a ca. 0.268 nm lattice spacing indexed to the {3 1 −3} facets of TiO_2-B can also be observed in certain areas. These line defects and lattice rotation may produce deep energy level which could become combination centers to capture photogenerated electrons and holes [24]. As a result, vanishing of the long-range order in TNB may result in a poor activity in contrast to that in ANB.

The UV–vis diffused-reflectance spectra (DRS) of different TiO_2 nanobelts and P25 nanoparticles are shown in Fig. 4a. A slightly blue shift of the absorption onset takes place in ANB compared with TNB, while the P25 present a red shift relative to both nanobelts. Using the Tauc equation, their band gaps are calculated, and the resulted plots of $(Ahv)^{1/2}$ versus hv are displayed in Fig. 4b. The indirect band gap values for ANB, TNB and P25 are ca. 3.0, 2.92 and 2.8 eV, respectively. It is accessible that the broadening of band gap from TNB to ANB is originated from the sharply reduced amount of TiO_2-B in ANB. Because the band gap of pure TiO_2-B nanobelts (2.8 eV) is lower than the anatase nanobelts (3.1 eV) [9]. The existence of lattice defects, including crystal mismatching and color centers, may

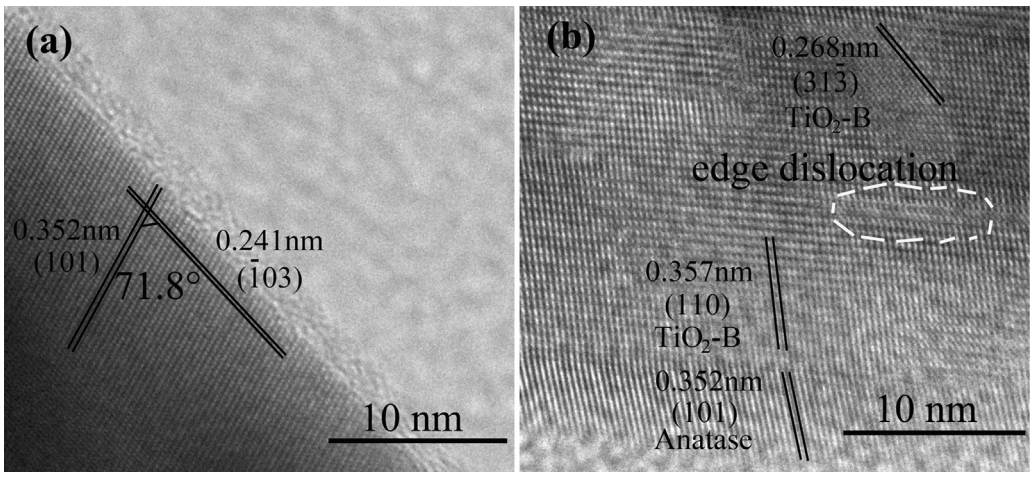

Fig. 3. Typical HRTEM images of ANB (a) and TNB (b).

be another reason of the lowered band gap for TNB [25,26]. Meanwhile, due to the particular quasi-1D nanostructure and the still low content of TiO_2-B, the band gap energy about 3.0 eV of ANB is less than the bulk anatase (3.2 eV). In addition, the narrow energy gap of rutile and the specific heterostructure of bicrystal could account for the red shift of P25 nanoparticles [27]. All the DRS results can further evidence that crystalline improvement by the introduction of ethanol treatment during the procedure.

The related photocatalytic activities of different samples were evaluated by degradation of Rhodamine-B (RB) under ultraviolet light, and the results are shown in Fig. 5a. It is clear that the ethanol treated TiO_2 nanobelts (ANB) exhibit a much higher degradation ratio in 60 min. compared to the untreated nanobelts (TNB), which are 73% and 36%, respectively. Furthermore, the degradation ratio of ANB even exceeds the P25 reaction system (67%), while the activity of the acid-treated TiO_2 nanobelts (H-TNB) with a degradation ratio of 51.5% is still not as good as P25, matching very well to previous results [18–20]. The reaction rate constants (K) of different samples are calculated by using the first-order

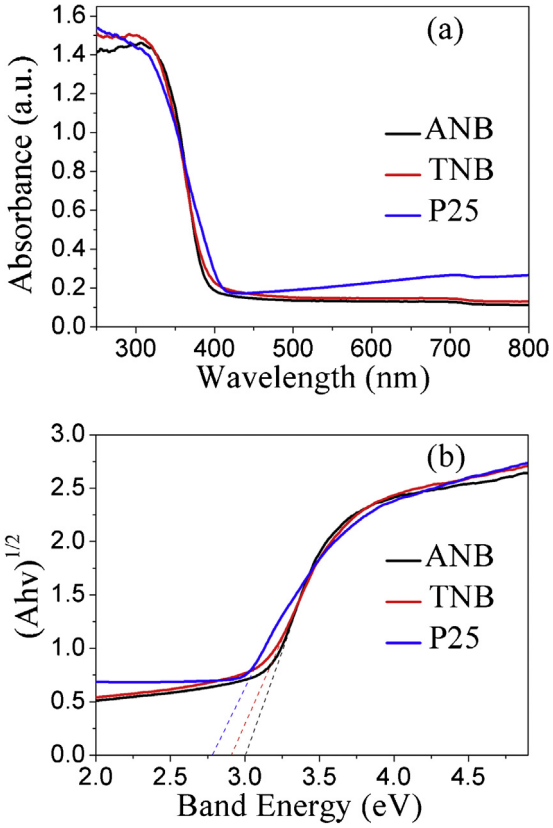

Fig. 4. UV–vis DRS (a) and the plots of $(Ahv)^{1/2}$ vs. hv (b) for ANB, TNB and P25. (For interpretation of the references to color in this figure legend, the reader is referred to the web version of this article.)

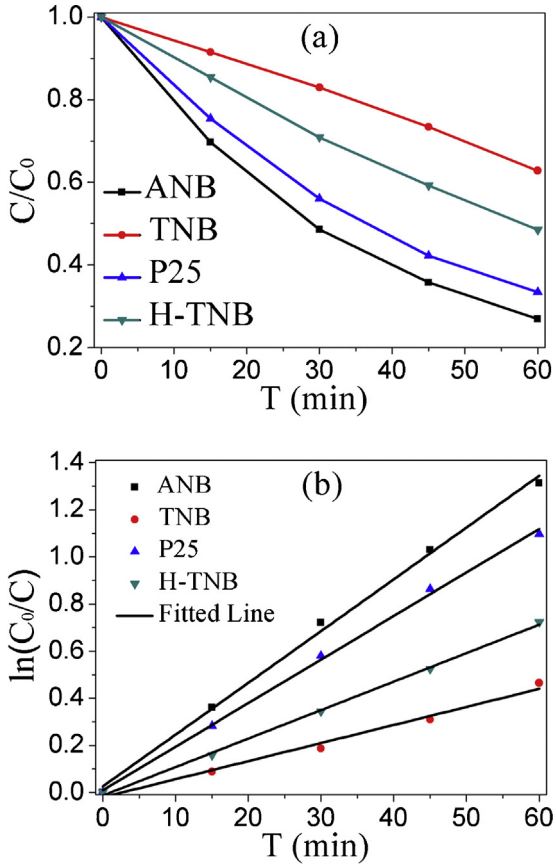

Fig. 5. Time courses for photocatalytic degradation of Rhodamine-B under UV light by different TiO_2 photocatalysts (a); the plots of $\ln(C_0/C)$ as a function of radiation time for the corresponding TiO_2 system (b).

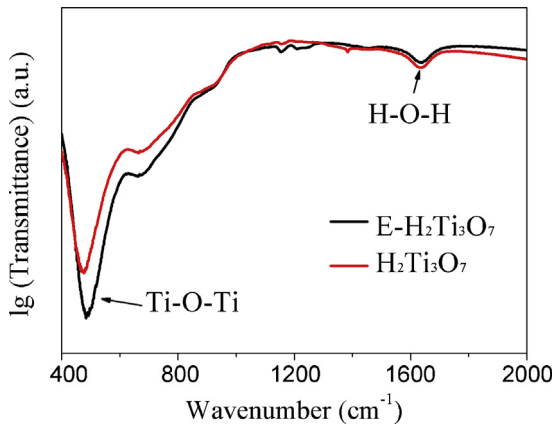

Fig. 6. FT-IR spectra of E-$H_2Ti_3O_7$ and $H_2Ti_3O_7$, the ordinate denotes the common logarithm (log) of transmittance values. (For interpretation of the references to color in this figure legend, the reader is referred to the web version of this article.)

dynamic equation: $\ln(C/C_0) = Kt$, where t is the reaction time, and C/C_0 denotes the concentration change of RB solution. The plots of $\ln(C/C_0)$ versus t are displayed in Fig. 5b, and the slopes of fitted lines stand for the values of K, which are equal to 0.022, 0.0077, 0.0185 and 0.0121 min^{-1} for ANB, TNB, P25 and H-TNB, respectively. These data demonstrate that the ethanol treatment of the as-prepared $H_2Ti_3O_7$ nanobelts can lead to a substantial progress in the photocatalytic activity. Considering the obvious BET distinction of different samples, we further calculate the essential reaction activity rates (K_0) of different TiO_2 photocatalysts, which can be expressed as: $K_0 = K/S_{bet}$ (Table 1). We can see that the K_0 value of ANB is much higher than that of TNB, H-TNB and P25. The result reflects that the better anatase crystallinity induces the much improved photocatalytic efficiency of ANB. Moreover, the band gap broadening of ANB which results in high reactive electron–hole pairs may also contribute to the boost of photocatalytic activity.

All the above characterizations consistently prove the improved changes in phase and crystallinity due to the introduction of ethanol. Zhou et al. reported that the phase of TiO_2-B in the nanobelts transformed into anatase completely at temperature higher than 800 °C, owing to the similar lattice structure between TiO_2-B and as-prepared $H_2Ti_3O_7$, as well as the shape limit effects in nanobelts [9]. In our case here, the transformation temperature decreases after the ethanol treatment. In order to clarify the atomic bonding state of the samples before calcination, both original $H_2Ti_3O_7$ and the ethanol treated $H_2Ti_3O_7$ were investigated by the Fourier transform infrared spectroscopy (FT-IR) in the range of 400–2000 cm^{-1}. As illustrated in Fig. 6, both spectra exhibit an absorption peak around 1635 cm^{-1}, which corresponded to the bending vibration of H—O—H [28]. Meanwhile, vibration around 897 cm^{-1}, which represents the stretching vibration of short Ti—O bonds involving nonbridging oxygen coordinated with sodium ions, was not observed [29]. These results signify the existence of hydrogen and lack of sodium ions in both samples after the acid washing. More importantly, the intensity of Ti—O—Ti vibration mode around 490 cm^{-1} of E-$H_2Ti_3O_7$ is enhanced compared to the original $H_2Ti_3O_7$ [30]. That is to say, the introduction of ethanol indeed is in favor of the bonding formation between titanium and oxygen atoms. Thus, the emergence of ANB may be depicted as follows: the quasi-1D $Na_xH_{2-x}Ti_3O_7$ nanobelts are firstly gained through the hydrothermal reaction. The $Na_xH_{2-x}Ti_3O_7$ nanobelts are composed of [TiO_6] octahedra with shared edges and vertices which the Na^+ and H^+ cations are embedded in the interlayer space. The subsequent soaking in dilute HCl aqueous solution promotes the formation of $H_2Ti_3O_7$ nanobelts by ion exchange. Then the ethanol treatment lead the chelation between the deprotonated alcohol ligands and titanium ions in the [TiO_6] octahedral [31]. Through this process, a new type of E-$H_2Ti_3O_7$ possesses a new crystalline structure and an enhanced bonding intensity between Ti and O atoms may form, which is apt to transform to anatase in the following lattice distortion and recrystallization compared with the as-prepared $H_2Ti_3O_7$. At the same time, the confinement originated from the structural similarity is destroyed, which leads to the irregular edges of ANB through the electron microscope observation. As a result, the phase transformation of TiO_2-B to anatase is much easier to realize.

4. Conclusion

In summary, a new method of ethanol treatment was developed to synthesize TiO_2 nanobelts. The ethanol treated ANB exhibits a significant improvement in crystallinity of anatase and severely reduced amount of TiO_2-B compared with the untreated TiO_2 nanobelts (TNB). A much higher photocatalytic activity of ANB in degradation Rhodamine-B under ultraviolet light can be obtained if comparing to TNB. Although the detailed mechanism of the crystalline change by the ethanol treatment is still not clear, the method can be a good candidate for many future applications, including the photocatalyst materials.

Acknowledgements

This work was supported by the National Basic Research Program of China (2012CB922000) and the Fundamental Research Funds for the Central Universities. Prof. Lu also thanks the support from the US Air Force Office of Scientific of Research (AFOSR).

References

[1] H. Yu, J. Yu, B. Cheng, S. Liu, Nanotechnology 18 (2007) 065604.
[2] A. Fujishima, T.N. Rao, D.A. Tryk, Journal of Photochemistry and Photobiology C: Photochemistry Review 1 (2000) 1–21.
[3] H. Liu, X. Dong, G. Li, X. Su, Z. Zhu, Applied Surface Science 271 (2013) 276–283.
[4] L. Qi, Y. Liu, C. Li, Applied Surface Science 257 (2010) 1660–1665.
[5] D. Wang, D. Choi, Z. Yang, V.V. Viswanathan, Z. Nie, C. Wang, Y. Song, J.-G. Zhang, J. Liu, Chemistry of Materials 20 (2008) 3435–3442.
[6] M. Kitta, T. Akita, Y. Maeda, M. Kohyama, Applied Surface Science 258 (2012) 3147–3151.
[7] A. Fujishima, K. Honda, Nature 238 (1972) 37–38.
[8] M.A. Khan, H.-T. Jung, O.-B. Yang, Journal of Physical Chemistry B 110 (2006) 6626–6630.
[9] W. Zhou, L. Gai, P. Hu, J. Cui, X. Liu, D. Wang, G. Li, H. Jiang, D. Liu, H. Liu, CrystEngComm 13 (2011) 6643–6649.
[10] Y. Wang, G. Du, H. Liu, D. Liu, S. Qin, N. Wang, C. Hu, X. Tao, J. Jiao, J. Wang, Advanced Functional Materials 18 (2008) 1131–1137.
[11] N. Wu, J. Wang, D.N. Tafen, H. Wang, J.-G. Zheng, J.P. Lewis, X. Liu, S.S. Leonard, A. Manivannan, Journal of the American Chemical Society 132 (2010) 6679–6685.
[12] T. Kasuga, M. Hiramatsu, A. Hoson, T. Sekino, K. Niihara, Advanced Materials 11 (1999) 1307–1311.
[13] V. Štengl, S. Bakardjieva, J. Šubrt, E. Večerníková, L. Szatmary, M. Klementová, V. Balek, Applied Catalysis B: Environmental 63 (2006) 20–30.
[14] L. Zhu, L.X. Cao, G. Su, W. Liu, L. Song, H. Liu, B.H. Dong, Applied Surface Science 257 (2011) 7932–7937.
[15] Y. Bai, W. Li, C. Liu, Z. Yang, X. Feng, X. Lu, K.-Y. Chan, Journal of Materials Chemistry 19 (2009) 7055–7061.
[16] R. Marchand, L. Brohan, M. Tournoux, Materials Research Bulletin 15 (1980) 1129–1133.
[17] T. Ohno, K. Sarukawa, M. Matsumura, Journal of Physical Chemistry B 105 (2001) 2417–2420.
[18] W. Zhou, G. Du, P. Hu, G. Li, D. Wang, H. Liu, J. Wang, R.I. Boughton, D. Liu, H. Jiang, Journal of Materials Chemistry 21 (2011) 7937–7945.
[19] R. Liu, P. Hu, S. Chen, Applied Surface Science 258 (2012) 9805–9809.
[20] W. Zhou, G. Du, P. Hu, Y. Yin, J. Li, J. Yu, G. Wang, J. Wang, H. Liu, J. Wang, Journal of Hazardous Materials 197 (2011) 19–25.
[21] L. Chen, F. Li, B.B. Ni, J. Xu, Z.P. Fu, Y.L. Lu, RSC Advances 2 (2012) 10057–10063.
[22] Z. Yanqing, S. Erwei, C. Zhizhan, L. Wenjun, H. Xingfang, Journal of Materials Chemistry 11 (2001) 1547–1551.
[23] M. Wei, Y. Konishi, H. Zhou, H. Sugihara, H. Arakawa, Chemical Physics Letters 400 (2004) 231–234.
[24] V.N. Kuznetsov, N. Serpone, Journal of Physical Chemistry C 113 (2009) 15110–15123.

[25] D. Li, N. Ohashi, S. Hishita, T. Kolodiazhnyi, H. Haneda, Journal of Solid State Chemistry 178 (2005) 3293–3302.
[26] Y.Z. Li, N.H. Lee, E.G. Lee, J.S. Song, S.J. Kim, Chemical Physics Letters 389 (2004) 124–128.
[27] P.Y. Dong, B. Liu, Y.H. Wang, L.N. Guo, Y.J. Huang, S. Yin, Journal of the Electrochemical Society 158 (2011) K183–K186.
[28] M. Qamar, C.R. Yoon, H.J. Oh, N.H. Lee, K. Park, D.H. Kim, K.S. Lee, W.J. Lee, S.J. Kim, Catalysis Today 131 (2008) 3–14.
[29] G.D. Sheng, H.P. Dong, R.P. Shen, Y.M. Li, Chemical Engineering Journal 217 (2013) 486–494.
[30] H. Yin, Y. Wada, T. Kitamura, S. Kambe, S. Murasawa, H. Mori, T. Sakata, S. Yanagida, Journal of Materials Chemistry 11 (2001) 1694–1703.